Published in final edited form as:
J Neurosci Methods. 2010 August 30; 191(2): 158–165. doi:10.1016/j.jneumeth.2010.06.015.

Identification of Neuromuscular Junctions by Correlative Confocal and Transmission Electron Microscopy

Shannon Modla[1], **Janet Mendonca**[2,3], **Kirk J. Czymmek**[1,2], and **Robert E. Akins**[3]

[1] Delaware Biotechnology Institute Bio-Imaging Center, University of Delaware

[2] Department of Biological Sciences, University of Delaware

[3] Department of Biomedical Research, A. I. duPont Hospital for Children

Abstract

The physiological processes regulating neuromuscular transmission are highly dependent on the structural features of the motor neuron and motor endplate, and detailing the structure of neuromuscular junctions (NMJs) in muscle biopsies is a powerful method for research and diagnostics. The observation of NMJ ultrastructure, however, is complicated by the difficulty in locating NMJs for analysis by electron microscopy. Consequently, a correlative confocal-transmission electron microscopy method was developed. Fixed muscle samples were cryo-protected in sucrose, sectioned on a cryostat, and stained with fluorescent α-bungarotoxin for confocal microscopy. Sections containing junctions were mapped and then processed for transmission electron microscopy (TEM). Cryostat sections allowed large expanses of muscle tissue to be rapidly screened and enabled specific junctions to be targeted for TEM. The morphology of the junctions was well preserved with all essential features of the pre- and postsynaptic elements readily identifiable without freeze-damage. Unlike NMJ correlative methods using histochemical stains and DAB photo-oxidation, no electron dense precipitate was deposited over the NMJ, enabling an unobstructed view of the pre- and postsynaptic structures.

Keywords

neuromuscular junction; correlative microscopy; confocal microscopy; transmission electron microscopy

Corresponding author: Kirk Czymmek, Delaware Biotechnology Institute, 15 Innovation Way, Suite 117, University of Delaware, Newark, DE 19711 USA, Telephone: (302) 831-3450, Fax: (302) 831-4841, kirk@udel.edu.
Shannon Modla
Delaware Biotechnology Institute, 15 Innovation Way, Suite 117, University of Delaware, Newark, DE 19711, USA
Janet Mendonca
Department of Biological Sciences, University of Delaware, Newark, DE 19716, USA
Dr. Kirk J. Czymmek
Delaware Biotechnology Institute, 15 Innovation Way, Suite 117, University of Delaware, Newark, DE 19711, USA
Dr. Robert E. Akins
Department of Biomedical Research, A. I. duPont Hospital for Children, 1600, Rockland Rd, Wilmington, DE 19803, USA

Introduction

The neuromuscular junction (NMJ) is the key functional unit that controls muscle contraction and consists of a specialized region along a muscle fiber whereby a motor neuron synapses with a muscle cell. In response to an action potential and subsequent cytoplasmic Ca^{+2} influx, a pool of synaptic vesicles within the motor neuron terminal fuse with the presynaptic membrane, in regions called active zones, and release the neurotransmitter acetylcholine into the synaptic cleft. Neurotransmitter diffuses across the synaptic cleft and interacts with the sarcolemma of the muscle cell, which is characterized by highly convoluted junctional folds. Acetylcholine binds to receptors at the apex of junctional folds (Fertuck and Salpeter, 1974; Flucher and Daniels, 1989), causing a conformational change of the acetylcholine receptor that forms a nonselective channel for cations to enter the muscle cell (Dwyer et al., 1980; Stoud et al., 1990). Subsequently, voltage-gated Na^{+} channels concentrated in the valleys of the junctional folds (Flucher and Daniels, 1989), trigger endplate depolarization. If the depolarization exceeds a certain threshold, an action potential fires, and a wave of depolarization propagates through the T-tubules and ultimately leads to muscle contraction.

The functional state of the NMJ is highly correlated to its ultrastructure, making morphological observations of the NMJ an important aspect of understanding its physiology. This structure-function relationship is most clearly demonstrated in cases where ultrastructural abnormalities in either the presynaptic motor neuron or postsynaptic muscle lead to pathophysiological conditions. For instance, in NMJ disorders such as auto-immune or congenital myasthenia gravis and Lambert-Eaton syndrome, the NMJs are altered in a number of ways that may include: reduced size (Hutchinson et al., 1993; Quiram et al., 1999), less elaborate junctional folds (Hutchinson et al., 1993; Quiram et al., 1999; Slater et al., 2006; Shiraishi et al., 2005), a loss of acetylcholine receptors (Engel et al., 1990; Slater et al., 2006), reduced number of synaptic vesicles (Engel et al., 1990; Walls et al., 1993), fewer calcium channels along the presynaptic membrane (Fukunaga et al., 1982), and reduced sodium channels within the valleys of the junction folds (Ruff and Lennon, 1998). The physiological consequences of these abnormalities essentially reduce the safety factor of neuromuscular transmission, greatly decreasing the probability of a muscle end-plate action potential (Wood and Slater, 2001). Abnormalities of the NMJ have also been demonstrated in more common diseases such as diabetes mellitus. In mice with induced diabetes, the motor neurons had fewer synaptic vesicles, atypical mitochondria, and myelin figures and in the muscle cells, there were swollen mitochondria, increased glycogen granules, and irregular T-tubules relative to normal mice. Such observations were correlated with a reduced motor endplate potential and resting membrane potential (Fahim et al., 2000).

Morphological studies at the resolution provided by transmission electron microscopy (TEM) have complimented electrophysiological and genetic approaches to understanding the underlying mechanisms of normal and abnormal neuromuscular transmission. Transmission electron microscopy is a valuable tool in the study of NMJs because it allows the microanatomy of the pre- and postsynaptic elements to be imaged at a resolution greatly exceeding conventional light microscopy. However, NMJs tend to be organized in specific bands throughout the muscle rather than homogeneously distributed (Ma et al., 2002). This makes locating NMJs from a random muscle biopsy for TEM problematic. Reliable means to locate NMJs for ultrastructural analysis using straightforward methodology would greatly improve the utility of TEM in research and clinical diagnostics of NMJ-associated diseases. Therefore, we have a developed a simple correlative method that allows NMJs to be first screened, identified and mapped by conventional fluorescence or confocal microscopy and subsequently imaged by TEM. This method can be used with precious tissue biopsies to

efficiently maximize the recovery of NMJs for TEM and facilitate the study of NMJs in both diseased and normal states.

Materials and Methods

Confocal Microscopy

Samples were processed according to the schematic depicted in Fig. 1. Briefly, adult female rats were euthanized by CO_2 inhalation under an IACUC approved protocol (Akins) and muscle from the diaphragm and leg was immediately excised into 4% paraformaldehyde in 0.1M Sorensen's phosphate buffer pH 7.2. The muscles were cut into 1 mm × 2 mm pieces and held in fixative for further processing. The muscle tissue was rinsed 3×, 15 min each, in 0.1 M phosphate buffer and gradually infiltrated on a rotator at room temperature with 2.3 M sucrose: 0.1 M phosphate buffer (1:3, 1:2, 1:1, 2:1, 3:1; 1 h each) followed by two changes in 2.3 M sucrose, 1 h each, and overnight in fresh 2.3 M sucrose. Multiple bundles of cryo-protected muscle were oriented longitudinally in a disposable base mold (Cat No 62534, EMS, Hatfield, PA), excess sucrose was removed with filter paper and the muscle was embedded in Tissue Freezing Medium ™ (Cat No 72592, EMS, Hatfield, PA) and frozen in a Leica CM3050 S cryostat. Ten micron thick longitudinal sections were cut at a chamber temperature and object temperature of −30°C and collected onto cold adhesive microscope slides (Cat No 62800-4X, EMS, Hatfield, PA) using the CryoJane® Tape-Transfer System (Instrumedics, Inc., St Louis MO). The sections were brought to room temperature and held in PBS until they were stained with α-bungarotoxin-AlexaFlour™ 555 for up to 1 h. The sections were rinsed 3x, 10 min each, with PBS, mounted in PBS with a 22×40 coverslip, and tile scanned on a Zeiss LSM510 confocal microscope with a HeNe 543 nm laser and 560 nm long pass emission filter set using a 10x C-Apochromat water immersion lens (Numerical Aperture 0.45). Confocal z-stacks were acquired with a 40x C-Apochromat water immersion lens (Numerical Aperture 1.2) and rendered in Zeiss AIM VisArt software (Rel. 4.2). Slides were stored in PBS for TEM processing.

Transmission Electron Microscopy

Slides containing NMJs were fixed overnight at 4°C in 2% glutaraldehyde and 2% paraformaldehyde in 0.1 M sodium cacodylate buffer pH 7.4. The sections were rinsed 3x, 15 min each, in 0.1 M sodium cacodylate buffer and fixed for 2 h in 1% osmium tetroxide in buffer. Following two buffer and two water washes, the slides were dehydrated in a graded ETOH series (25%, 50%, 75%, 95%, 100%, 100%; 15 min each) and infiltrated with Embed-812 resin: 100% ETOH (1:3, 1:2, 1:1, 2:1, 3:1; 1 h each). After two changes in 100% Embed-812, the slides were infiltrated overnight in fresh 100% resin. Slides were placed into fresh resin for 1 h, excess resin was drained from the slides and the sections were inverted onto resin-filled slide-duplicating molds (Cat No 10545, Ted Pella, Redding, CA). The sections polymerized in an oven at 60°C for 48 h. Regions of interest were identified from confocal tiles and isolated from the rest of the slide by chipping away excess glass with a diamond scribe. The sample was mounted glass-side down onto a pre-polymerized resin BEEM capsule using super glue. A block face was trimmed to encompass an area containing multiple NMJs using the confocal tile scans as a reference. An image of the final block face was taken with a Zeiss M^2BIO dissecting microscope equipped with a Zeiss Axiocam (Fig. 4C) and used to further refine the size of the trapezoid. Alternating sets of ultrathin (60–70 nm) and semithin (200 nm) sections were collected with a Reichert-Jung Ultracut E ultramicrotome. Semithin sections were dried onto glass slides, stained with epoxy tissue stain (Cat No 14950 EMS, Hatfield, PA) and imaged with a Zeiss Axioskop 2 equipped with a Zeiss Axiocam. The semithin sections in conjunction with the image of the resin block face served as references to identify the same muscle fibers by TEM that had been previously imaged by confocal microscopy. Ultrathin sections were collected onto 200 mesh

formvar-carbon coated copper grids and stained with methanolic uranyl acetate and Reynolds lead citrate (Reynolds, 1963). Samples were viewed with a Zeiss 902 CEM at 80kV or a Zeiss Libra 120 at 120kV, and images were captured with an Olympus Soft Imaging System Megaview II or Gatan Ultrascan 1000 digital cameras, respectively.

To ensure no deleterious effects of sucrose infiltration to tissue morphology, control samples were processed as follows. An adult male Sprauge-Dawley rat was sacrificed under an IACUC approved protocol and the diaphragm with dissected into 4% paraformaldehyde in 0.1 M Sorensen's phosphate buffer pH 7.2 and cut into 1 mm × 2 mm pieces. Tissue was fixed at 4°C for four days and then washed 3×, 10 min each, with PBS, stained with α-bungarotoxin-AlexaFlour™ 555 for 1 h and then washed 3×, 10 min each, in PBS. Muscle pieces were imaged on a Zeiss LSM 510 confocal with a HeNe 543 nm laser and 560 nm long pass emission filter set using a 10x C-Apochromat water immersion lens (Numerical Aperture 0.45). Pieces of muscle containing a dense population of NMJs were fixed in 2% glutaraldehyde and 2% paraformaldehyde in 0.1M sodium cacodylate buffer and then processed for TEM as described above for the sucrose-protected muscle sections.

Processing of Human Biopsies

To demonstrate the applicability of this technique for human NMJs, human muscle samples were collected after obtaining IRB approval for the study and written consent and assent. The patient was selected randomly from a population undergoing spinal fusion surgery for idiopathic scoliosis. A biopsy (approximately 1 cm^3) was taken from the lateral aspect of the spinalis at the thoraco-lumbar junction on the concave side of the spinal curve. Immediately following surgical excision, the sample was placed into freshly-prepared 4% paraformaldehyde in 0.1M Sorensen's phosphate buffer pH 7.2. The material was transferred to the lab where it was cut into smaller, 1×2mm pieces and placed in fresh 4% paraformaldehyde in 0.1M Sorensen's phosphate buffer overnight. The samples were processed for confocal screening and TEM as described above for the rat tissues.

Image Processing for Overlay

Confocal and TEM image files were imported into Adobe Photoshop CS3 and processed according to Keene et al. (2008). An optical slice from the confocal Z-stack was copied and pasted as a separate layer onto the corresponding TEM micrograph, and the opacity of the confocal selection was reduced to ~35% to see the underlying TEM micrograph. The free transform tool was used to resize and rotate the confocal selection so that the signal overlaid with the junctional folds in the TEM micrograph.

Results

Following tissue preparation, NMJ screening and subsequent processing for TEM (Fig. 1) revealed that the rat NMJ was well preserved without apparent artifact from the sucrose infiltration and freezing used in sample processing (Fig. 2). All morphological features of the motor neuron and myocyte including the synaptic vesicles, junctional folds, basal lamina of the sarcolemma, myofilaments, neurofilaments, mitochondria, and pre- and postsynaptic membranes were readily identifiable with little ultrastructural artifacts and no detectable freeze damage (Figs. 2, 5C & 6A). The appearance of the pre- and postsynaptic membranes of both control (Fig. 2A) and sucrose-protected (Fig. 2B) rat tissue varied depending on the plane of the section. Membranes appeared distinct when cut in the plane of the section and less defined when sectioned obliquely (Fig. 2). The quality of ultrastructural preservation of the sucrose-protected NMJs (Fig. 2B) was comparable to the non-sucrose protected control (Fig. 2A). Some evidence of extraction was apparent along the myelin sheaths, but this was observed in both the sucrose-protected and non-sucrose protected control muscles.

For human tissues, NMJs were found with the same efficiency as for the rat tissues. Ten human patient biopsies were collected and processed in the same manner as rat tissues, and in all patients, NMJs were readily identified. As in rat tissues, all elements of the motor neuron and myocyte were identifiable with good ultrastructural preservation (Fig. 3).

By confocal microscopy, NMJs appeared as brightly fluorescent convoluted and ovoid structures representing the junctional folds juxtaposed to the surface of muscle fibers. When present, multiple NMJs often appeared in a single cryo-section (Fig. 4A), potentially allowing specific junctions and those of a particular orientation to be selected for transmission electron microscopy. Longitudinally sectioned muscle fibers allowed NMJs to be located more efficiently than transverse sections. A three-dimensional reconstruction (Fig. 4B and Fig. 4B–3Dmovie) from confocal z-stack (Fig. 4B–Zmovie) revealed the three-dimensional arrangement of the NMJ complex, with the α-bungarotoxin staining limited to the surface of the motor endplate. This 3D confocal perspective was especially valuable when interpreting TEM NMJs since only a very small fraction of the NMJ is visible by TEM.

To extend the correlation further, individual confocal optical slices were directly overlaid onto corresponding TEM image planes of targeted NMJs, thereby allowing a direct correlation between light and electron microscopy of the same structure (Figs. 5A–5D). In order to facilitate matching the appropriate confocal and TEM sections, we found it very useful to increase the brightness and contrast in the original confocal z-slice (Fig. 5A) so that the muscle fibers and other cytoplasmic details were visible as landmarks (Fig. 5B). Closer inspection of an NMJ confocal/TEM overlaid image (Fig. 6B) from a portion of Fig. 5D (black box), reveals the good correlation of the α-bungarotoxin fluorescence (red) with the junctional folds and allows unobscured visualization of morphological features of the raw TEM data (Fig. 6A).

Discussion

Rat skeletal muscle was used as a model to develop a correlative technique for identifying NMJs by confocal and transmission electron microscopy. Muscle samples were gently fixed to maintain probe or antibody affinity and minimize autofluorescence and then cryo-protected in sucrose to prevent ice crystal formation during subsequent cryostat sectioning. Semi-thick sections (~10 microns) were suitable for good probe penetration for optical microscopy and to have sufficient material with negligible artifact at the cut interfaces or at the adhesive/slide interface used to maintain tissue through subsequent processing. Sections were screened for NMJs by confocal microscopy and then further processed for transmission electron microscopy.

The ultrastructural preservation of the motor neuron and its associated muscle fiber was maintained despite exposure to a high sucrose gradient, freezing, and post-processing. Sucrose is a commonly used cryoprotectant that is employed by the Tokuyasu method of cryoultramicrotomy for immunogold labeling of ultrathin sections (Tokuyasu, 1973). Similar to the results with α-bungarotoxin reported here, Keller et al. (1984) showed that sucrose-protected ultrathin cryosections could be immunogold labeled and then post-fixed in osmium, dehydrated, and embedded in resin. The morphology of such preparations was equivalent to conventionally processed samples. The current experiment demonstrates that relatively large expanses of muscle can be screened for features of interest by cryo-protection and cryostat sectioning without compromising ultrastructural integrity. However, like any study investigating the morphology of diseased NMJs, it is essential to run control muscle in parallel to rule out any possible structural changes or artifacts generated by sample processing. Due to our small probe size, our technique did not require

permeabilization steps that might include Triton or saponin. However, there is no fundamental reason why antibody labeling would be precluded from performing ultrasmall gold or FluoroNanogold and silver enhancement for correlative fluorescence and electron microscopy using the procedure described here.

The most common method to identify NMJs by both light and electron microscopy uses histochemical staining techniques targeted toward acetylcholinesterase activity. Some histochemical methods applied to both light and electron microscopic observation of NMJs include those described by Koelle and Friedenwald (1949), Karnovsky and Roots (1964), and Strum and Hall-Craggs (1982). In Koelle and Friedenwald's (1949) method, tissue is incubated with the substrate acetylthiocholine and reacts with copper glycinate in the presence of acetylcholinesterase to form copper thiocholine, which further is reacted with ammonium sulfide to yield an electron dense deposit of copper sulfide. Variations of this method have also used gold and lead ions as capture reagents (Davis and Koelle, 1967). Unlike Koelle and Friedenwald's (1949) method, Karnovsky and Roots (1964) employed a single-step method in which acetylthiocholine, copper sulfate, and potassium ferricyanide reacted in the presence of acetylcholinesterase to directly form a copper ferrocyanide precipitate. The method described by Strum and Hall-Craggs (1982) used an incubation solution of hexazotized pararosaniline and indoxyl acetate to form a more precise distribution of precipitate in the junctional folds. In all histochemical methods, an electron dense precipitate is deposited over the NMJ in the vicinity of cholinesterase activity.

Although histochemical techniques effectively delineate the location of NMJs, they have several limitations. Foremost, the histochemical reactions deposit an electron dense precipitate over the NMJs that can obscure the underlying ultrastructural details, reduce morphological preservation, and limit resolution. Incubation times in the reaction medium need to be adjusted to compromise between visibility of the neuromuscular junction by light microscopy and decreased resolution at the level of electron microscopy. Moreover, the components of the reaction medium exhibit limited penetration into tissue, and staining is restricted to superficial muscle fibers (Davis and Koelle, 1967; Strum and Hall-Craggs, 1982). Lastly, the reaction product has the potential to diffuse away from the source of staining (Koelle and Friedenwald, 1949), and under certain conditions, the formation of needle-like crystals and nonspecific staining can occur (Karnovsky and Roots, 1964).

More recent techniques for correlating NMJs by confocal and transmission electron microscopy have used DAB photo-oxidation. When photo-bleached with intense epi-fluorescent illumination, certain fluorescent dyes release reactive oxygen species that oxidize diaminobenzidine (DAB) to form an electron dense precipitate (Deerink et al., 1994). DAB photo-oxidation of NMJs has been accomplished with the dye FM1-43 to demonstrate synaptic vesicle uptake at the motor neuron (Henkel et al., 1996; Teng and Wilkinson, 2000) and also with DiI or DiO by iontophoretic labeling (Gan et al., 1999; Bishop et al., 2004). As with histochemical staining of the NMJ, DAB photo-oxidation techniques also rely on the deposition of an electron dense reaction product to locate junctions by light and electron microscopy. However, the resulting reaction product is finer than those produced by histochemical methods and highly localized to the site of dye labeling. Drawbacks to DAB photo-oxidation methods include the nonspecific photo-conversion of endogenous peroxidases (Deerink et al., 1994). Moreover, FM1-43 uptake must occur in unfixed, electrically stimulated muscle fibers (Henkel et al., 1996), which is unsuited for fixed muscle biopsies. Lastly, iontophoretic labeling with DiO and DiI requires the injection of a dye crystal directly into individual NMJs and does not broadly label all NMJs within a sample for gross screening.

The use of sucrose-protected cryostat sections of muscle biopsies labeled with fluorescent α-bungarotoxin overcomes several limitations of histochemical acetycholinesterase staining and DAB photo-oxidation techniques for the direct correlation of NMJs by confocal and transmission electron microscopy. Cryostat sections allow large expanses of muscle tissue to be efficiently screened and mapped so that a significant fraction of junctions can be identified for transmission electron microscopy, permitting maximum utilization of often precious muscle biopsies. Moreover, the CryoJane® Tape-Transfer System used in conjunction with adhesive-coated slides allows flat, wrinkle-free sections to be collected that remain bonded to the slides throughout subsequent processing. Additionally, mapping of fluorescently labeled junctions with confocal tile scans allows junctions to be targeted for transmission electron microscopy without the introduction of an electron dense precipitate that can obscure underlying ultrastructural details. Efforts with non-sucrose protected muscle biopsies were technically possible when submerging tissue pieces in fluorescent tagged α-bungarotoxin. However, the probe only penetrated very near the cut surface, and this not only increased the likelihood that NMJs had mechanical damage but also any NMJs interior from the surface were not detectable. It must be noted that current enzymatic or photochemical electron dense reaction products will inherently have better correlative spatial resolution when compared to our described overlay method. This is due to the use of photon based detection method of light microscopy which has a diffraction limited lateral resolution of ~200 nanometers when using visible light. Although not widely available, it is certainly conceivable that refinement of this technique to overlay antibody or fluorescence protein based super-resolution techniques (Chi, 2009) will allow lateral resolution on the order of 20nm.

Although this method was highly effective at efficiently locating NMJ in tissue blocks for subsequent high resolution imaging, some slight modifications in the technique may further streamline data acquisition and facilitate image correlation. One such improvement is the use of adhesive-coated Permanox™ slides with the CryoJane® Tape-Transfer System. Permanox™ slides exhibit no autofluorescence, are resistant to common chemicals used for TEM processing and also separate easily from polymerized resin by immersing the slides in liquid nitrogen. Using Permanox™ rather than glass slides would eliminate the danger associated with sectioning very near a glass surface with a diamond knife. Our studies tested adhesive coated Permanox™ slides to collect cryostat sections of sucrose-protected tissue, but we found that an oily residue on the slides interfered with confocal imaging of the fluorescently-labeled muscle fibers when slides were stored for prolonged periods in PBS (data not shown). An additional useful modification to this reported protocol would to include a nuclear or other counterstain with the fluorescent bungarotoxin. Labeling nuclei in addition to the NMJs would create conspicuous landmarks with the confocal images that could be easily identified in thin section TEM images and improve the ease of correlating between the two optical platforms.

The method utilized in this report holds great potential for studying difficult-to-locate NMJs in human biopsies. Indeed, data from our lab shows that we can obtain very similar results with human samples (Fig. 3). In some of the earliest work (De Harven and Cöers, 1959) to study human NMJ ultrastructure by TEM, localization of NMJs was achieved by making an incision to expose the muscle fascia and electrically stimulating the muscle using a cathode electrode. The excitability threshold of the endplate was measured as a distinguishing factor in comparison with the surrounding muscle tissue, and a 2–4 mm muscle biopsy was obtained. This would provide a higher chance of finding a NMJ but would still require large areas of muscle tissue to be scanned ultrastructurally. Muscle biopsy samples obtained during surgical procedures provide little control and time for such measurements described above. Our method provides the advantage of shorter screening time and increased

efficiency in accurately locating NMJs obtained from patients undergoing critical surgical procedures.

In this study, fluorescent alpha-bungarotoxin successfully labeled NMJs in 10 μm thick cryostat sections. Alpha-bungarotoxin is a small 74 amino acid peptide isolated from the venom of *Bungarus multicinctus* that binds specifically to acetylcholine receptors (Lee, 1972). One potential limitation of α-bungarotoxin is to reliably identify junctions in patients with severely reduced numbers of acetylcholine receptors. For such situations, it may be possible to use other fluorescent markers such as the ω-conopeptide derived from the venom of *Conus* snails (Clark et al., 1981), fasciculin derived from *Dendroaspis angusticeps* venom (Rodriguez-Ithurralde et al., 1983), or a fluorescent conjugate of the lectin DBA from the legume *Dolichos biflorus* (Sanes and Cheney, 1982). Fasciculin has been used in electron microscope autoradiography of NMJs (Anglister et al., 1998) while DBA specifically labels carbohydrate moieties along the synaptic cleft, junctional folds, and basal lamina. The synthetic analog of ω-conopeptide, SNX-260, has been shown to specifically label non-N type voltage-sensitive Ca^{+2} channels along the presynaptic membrane of the motor neuron (Sugiura et al., 1995). The applicability of ω-conopeptide, DBA, or fasciculin to the current method will need further investigation.

In conclusion, we describe a simple yet powerful technique to efficiently localize a structure of interest identified by light microscopy, in this case NMJs, for correlative high resolution transmission electron microscopy. The tedious nature and perhaps futility of random sectioning at the TEM level for difficult to obtain biopsy samples provided the impetus for us to develop an improved method. However, this technique certainly is neither limited to biopsies, nor NMJs and conceivably would be helpful in instances where searching for a rare structure or event is better suited for screening at the light microscopic level before attempting TEM. In this study, we took full advantage of the optical sectioning and improved resolution and contrast afforded by confocal microscopy to obtain a 3D perspective of the full targeted NMJ. We believe that this approach significantly augments any resolution detail obtained via TEM and allows the TEM data to be put into perspective due to inherent limitations (visualizing a 70nm slice from a 50 micron structure). Such a combinatorial correlative technique allows information to be collected in multiple modalities from an individual targeted structure in a way that transcends scale and is thus a valuable tool when exploring underlying pathologies. We must emphasize that while confocal microscopy provided unique capabilities/automation and facilitated certain aspects of this technique, it certainly is not an absolute requirement to locate NMJs. In fact, all screening can be easily done with conventional epifluorescence microscopes, which are far more available to many labs. Albeit with lower resolution, a single image with a low magnification objective lens can be used in place of the tile-scan montage and then higher magnification objectives used to target the structure of interest in more detail. Indeed, we also expect that any probes that are compatible with the initial paraformaldehyde fixation (i.e, antibodies, fluorescent affinity probes and green fluorescent protein-fusions) would be useful with similar efficacy.

Supplementary Material

Refer to Web version on PubMed Central for supplementary material.

Acknowledgments

The project described and DBI Bio-Imaging Core Facility usage was supported by Grant Number 2 P20 RR016472-09 under the INBRE Program of the National Center for Research Resources (NCRR), a component of the National Institutes of Health (NIH), NICHD - HD051738 (Akins) and Nemours Foundation (Akins). We would

like to thank Dr. Christopher Martens and Dr. David Edwards from the Department of Kinesiology & Applied Physiology at the University of Delaware for generously supplying rat tissue.

References

Anglister L, Eichler J, Szabo M, Haesaert B, Salpeter MM. ^{125}I-labeled fasciculin 2: A new tool for quantitation of acetylcholinesterase densities at synaptic sites by EM-autoradiography. J Neurosci Meth. 1998; 81:63–71.

Bishop DL, Misgeld T, Walsh MK, Gan W, Lichtman JW. Axon branch removal at developing synapses by axosome shedding. Neuron. 2004; 44:651–661. [PubMed: 15541313]

Chi KR. Super-resolution microscopy: breaking the limits. Nat Meth. 2009; 6(1):15–18.

Clark C, Olivera BM, Cruz LJ. A toxin from the venom of the marine snail *Conus geographus* which acts on the vertebrate central neurvous system. Toxicon. 1981; 19:691–699. [PubMed: 6895426]

Davis R, Koelle GB. Electron microscopic localization of acetylcholinesterase and nonspecific cholinesterase at the neuromuscular junction by the gold-thiocholine and gold-thiolacetic acid methods. J Cell Biol. 1967; 34:157–171. [PubMed: 6033530]

Deerink TJ, Martone ME, Lev-Ram V, Green DPL, Tsien RY, Spector DL, Huang S, Ellisman MH. Fluorescence photooxidation with eosin: A method for high resolution immunolocalization and *in situ* hybridization detection for light and electron microscopy. J Cell Biol. 1994; 126:901–910. [PubMed: 7519623]

De Harven E, Coërs C. Electron microscope study of the human neuromuscular junction. J Biophysic and Biochem Cytol. 1959; 6:7–10.

Dwyer TM, Adams DJ, Hille B. The permeability of the endplate channel to organic cations in frog muscle. J Gen Physiol. 1980; 75:469–492. [PubMed: 6247422]

Engel AG, Walls TJ, Nagel A, Uchitel O. Newly recognized congenital myasthenic syndromes: I. Congenital paucity of synaptic vesicles and reduced quantal release II. High conductance fast-channel syndrome III. Abnormal acetylcholine receptor (AChR) interaction with acetylcholine IV. AChR deficiency and short channel-open time. Prog Brain Res. 1990; 84:125–137. [PubMed: 2267290]

Fahim MA, Hasan MY, Alshuaib WB. Early morphological remodeling of neuromuscular junction in a murine model of diabetes. J Appl Physiol. 2000; 89:2235–2240. [PubMed: 11090573]

Fertuck HC, Salpeter MM. Localization of acetylcholine receptor by ^{125}I-labeled α-bungarotoxin binding at mouse motor endplates. P Natl Acad Sci USA. 1974; 71:1376–1378.

Flucher BE, Daniels MP. Distribution of Na^+ channels and ankyrin in neuromuscular junctions is complemenetary to that of acetylcholine receptors and the 43 kd protein. Neuron. 1989; 3:163–175. [PubMed: 2560390]

Fukunaga H, Engel AG, Osame M, Lambert EH. Paucity and disorganization of presynaptic membrane active zones in the lambert-eaton myasthenic syndrome. Muscle Nerve. 1982; 5:686–697.

Gan W, Bishop DL, Turney SG, Lichtman JW. Vital imaging and ultrastructural analysis of individual axon terminals labeled by iontophoretic application of lipophilic dye. J Neurosci Meth. 1999; 93:13–20.

Henkel AW, Lübke J, Betz WJ. FM1-43 dye ultrastructure localization in and release from frog motor nerve terminals. Proc Nat Acad Sci USA. 1996; 93:1918–1923. [PubMed: 8700859]

Hutchinson DO, Walls TJ, Nakano S, Camp S, Taylor P, Harper M, Groover RV, Peterson HA, Jamieson DG, Engel AG. Congenital endplate acetylcholinesterase deficiency. Brain. 1993; 116:633–653. [PubMed: 8390325]

Karnovsky MJ, Roots L. A “direct-coloring” thiocholine method for cholinesterases. J Histochem Cytochem. 1964; 12:219–221. [PubMed: 14187330]

Keene DR, Tufa SF, Lunstrum GP, Holden P, Horton WA. Confocal/TEM overlay microscopy: A simple method for correlating confocal and electron microscopy of cells expressing GFP/YFP fusion proteins. Microsc Microanal. 2008; 14:342–348. [PubMed: 18598569]

Keller GA, Tokuyasu KT, Dutton AH, Singer SJ. An improved procedure for immunoelectron microscopy: Ultrathin plastic embedding of immunolabeled ultrathin frozen sections. Proc Natl Acad Sci USA. 1984; 81:5744–5747. [PubMed: 6435119]

Koelle GB, Friedenwald JS. A histochemical method for localizing cholinesterase activity. Proc Soc Exp Biol. 1949; 70:617–622. [PubMed: 18149447]

Lee CY. Chemistry and pharmacology of polypeptide toxins in snake venoms. Annu Rev Pharmacol. 1972; 12:265–286. [PubMed: 4339019]

Ma J, Smith BP, Smith TL, Walker FO, Rosencrance EV, Koman A. Juvenile and adult rat neuromuscular junctions: Density, distribution, and morphology. Muscle Nerve. 2002; 26:804–809. [PubMed: 12451605]

Quiram PA, Ohno K, Milone M, Patterson MC, Pruitt NJ, Brendman JM, Sine SM, Engel AG. Mutation causing congenital myasthenia reveals acetylcholine receptor β/δ subunite interaction essential for assembly. J Clin Invest. 1999; 104:1403–1410. [PubMed: 10562302]

Reynolds ES. The use of lead citrate at high pH as an electron-opaque stain in electron microscopy. J Cell Biol. 1963; 17:208–212. [PubMed: 13986422]

Rodriguez-Ithurralde D, Silveira R, Barbeito L, Dajas F. Fasciculin a powerful anticholinesterase polypeptide from *Dendroaspis angusticeps*. Neurochem Int. 1983; 5:267–274. [PubMed: 20487949]

Ruff RL, Lennon VA. End-plate voltage-gated sodium channels are lost in clinical and experimental myasthenia gravis. Ann Neurol. 1998; 43:370–379. [PubMed: 9506554]

Sanes JR, Cheney JM. Lectin binding reveals a synapse-specific carbohydrate in skeletal muscle. Nature. 1982; 300:646–647. [PubMed: 7144916]

Shiraishi H, Matomura M, Yoshimura T, Fukudome T, Fukuda T, Nakao Y, Tsujihara M, Vincent A, Eguchi K. Acetylcholine receptors loss and postsynaptic damage in MuSK antibody-positive myasthenia gravis. Ann Neurol. 2005; 57:289–293. [PubMed: 15668981]

Slater CR, Fawcett PRW, Walls TJ, Lyons PR, Bailey SJ, Beeson D, Young C, Gardner-Medwin D. Pre- and post-synaptic abnormalities associated with impaired neuromuscular transmission in a group of patients with limb-girdle myasthenia. Brain. 2006; 129:2061–2076. [PubMed: 16870884]

Stoud RM, McCarthy MP, Shuster M. Nicotinic acetylcholine receptor superfamily of ligand-gated ion channels. Biochemistry-US. 1990; 29:11009–11023.

Strum JM, Hall-Craggs ECB. A method demonstrating motor endplates for light and electron microscopy. J Neurosci Meth. 1982; 6:305–309.

Sugiura Y, Woppmann A, Miljanich GP, Ko C. A novel ω-conopeptide for the presynaptic localization of calcium channels at the mammalian neuromuscular junction. J Neurocytol. 1995; 24:15–27. [PubMed: 7539483]

Teng H, Wilkinson RS. Clathrin-mediated endocytosis near active zones in snake motor boutons. J Neurosci. 2000; 20:7986–7993. [PubMed: 11050119]

Tokuyasu KT. A technique for ultracryotomy of cell suspensions and tissues. J Cell Biol. 1973; 57:551–565. [PubMed: 4121290]

Walls TJ, Engel AG, Nagel AS, Harper CM, Trastek VF. Congenital myasthenic syndrome associated with paucity of synaptic vesicles and reduced quantal release. Ann NY Acad Sci. 1993; 681:461–468. [PubMed: 8395161]

Wood SJ, Slater CR. Safety factor at the neuromuscular junction. Prog Neurobiol. 2001; 64:393–429. [PubMed: 11275359]

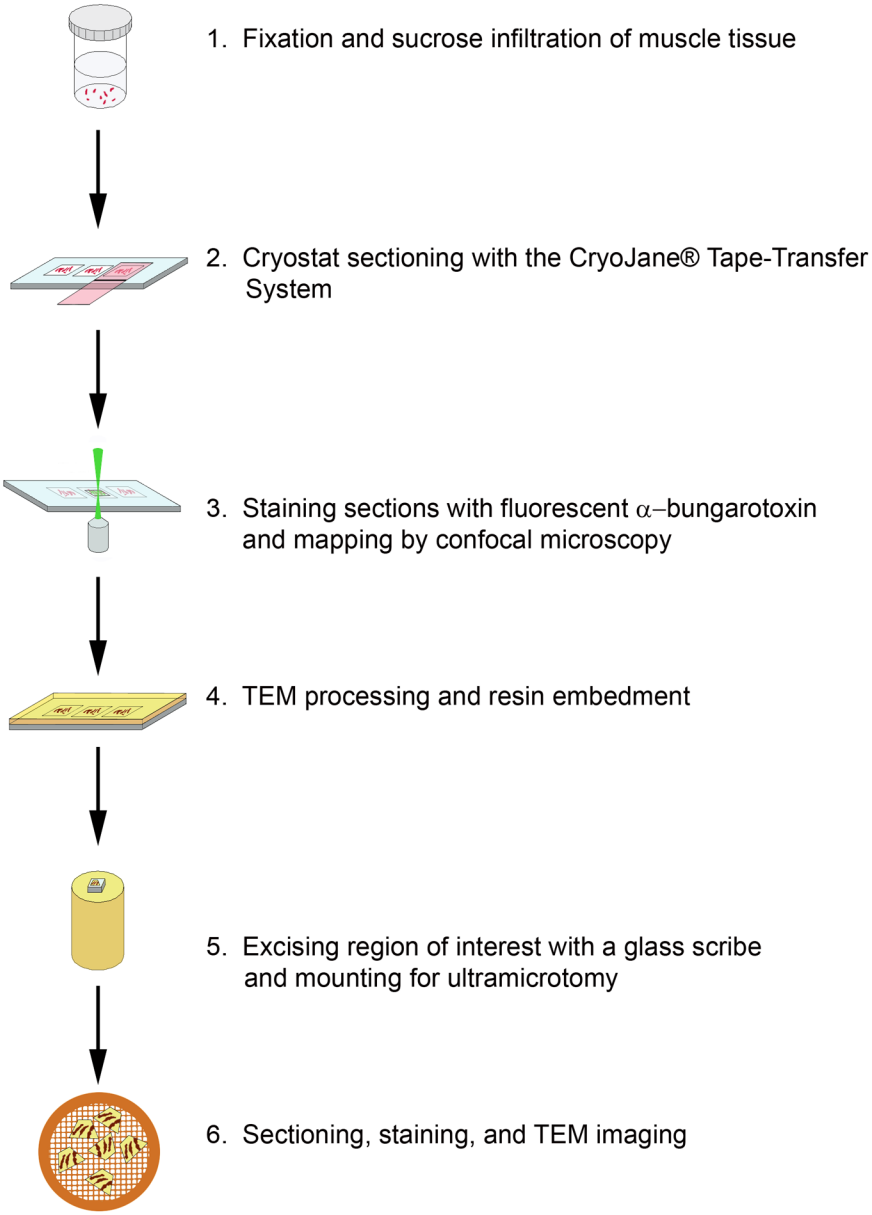

Figure 1.
Schematic illustrating the major steps involved in processing samples for correlative confocal-TEM imaging of sucrose-protected tissues.

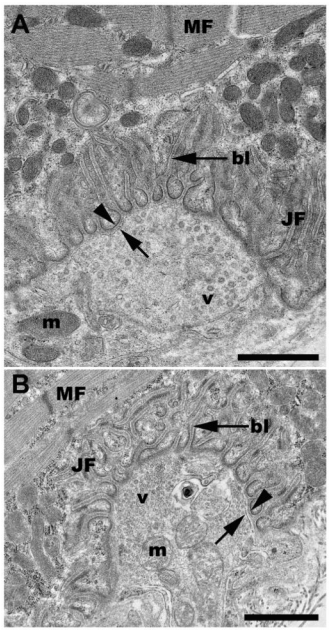

Figure 2.

Representative TEM micrographs of a neuromuscular junction from a control (2A) and a sucrose-protected rat muscle (2B). bl, basal lamina; JF, junctional folds; m, mitochondria; MF, myofibrils; v, vesicles; arrowhead, post-synaptic membrane; arrow, pre-synaptic membrane. Scale bars= 1μm.

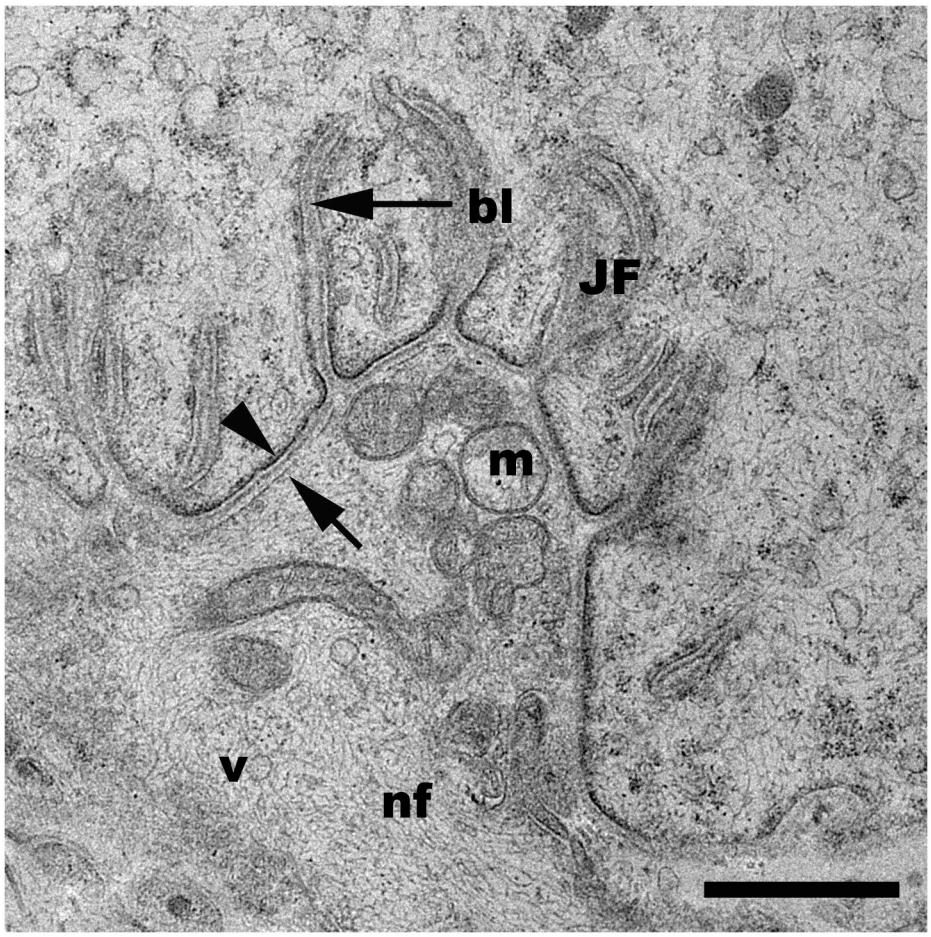

Figure 3.
Representative TEM micrograph of a neuromuscular junction from a human muscle biopsy. bl, basal lamina; JF, junctional folds; m, mitochondria; v, vesicles; arrowhead, post-synaptic membrane; arrow, pre-synaptic membrane. Scale bar= 1μm.

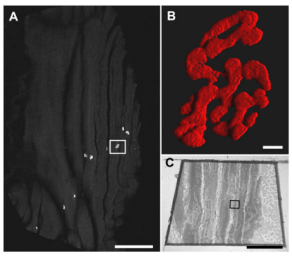

Figure 4.

A. Confocal tile scan of a 10 μm cryostat section of sucrose-protected rat muscle labeled with α-bungarotoxin-AlexaFlour™ 555. The boxed region was targeted for TEM. Scale bar = 500 μm. B. A high magnification three dimensional shadow projection rendering of the boxed NMJ in Fig. 4A. Scale bar= 5 μm. Movies of three-dimensional rendering (Fig. 4B-3Dmovie) and original confocal z-stack (Fig. 4B-Zmovie) available as supplementary data. C. Image of the resin block face. The boxed region corresponds to that in Fig. 4A. Scale bar= 500 μm.

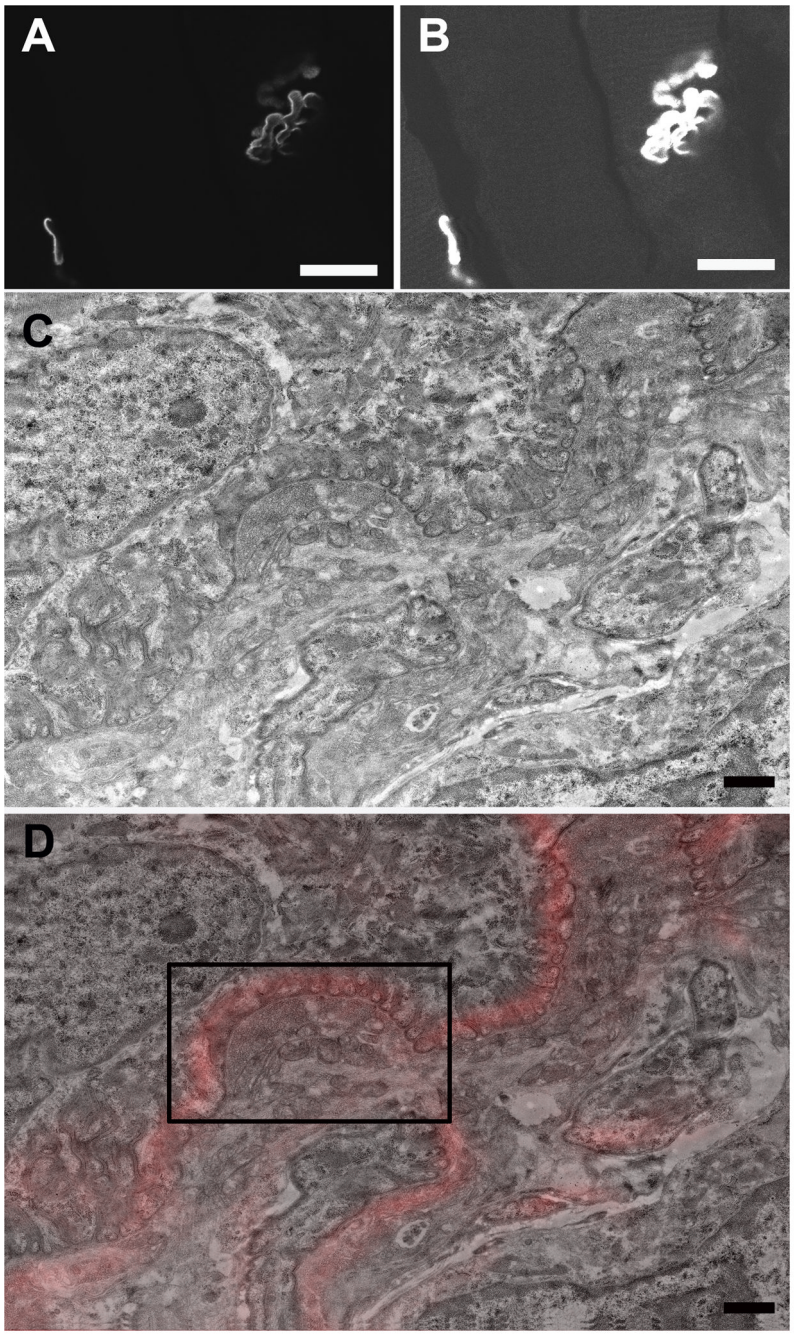

Figure 5.
A. A single slice from the confocal Z-stack of the NMJ depicted in Fig. 4B. Scale bar= 20 μm. B. Adjusting the brightness/contrast of Fig. 5A allowed muscle fibers to be visualized for correlation between confocal and TEM. Scale bar= 20 μm. C. Low magnification TEM montage of the NMJ depicted in Figs. 4A–B. Scale bar= 1 μm. D. TEM-confocal overlay of Fig 5C. Scale bar= 1 μm.

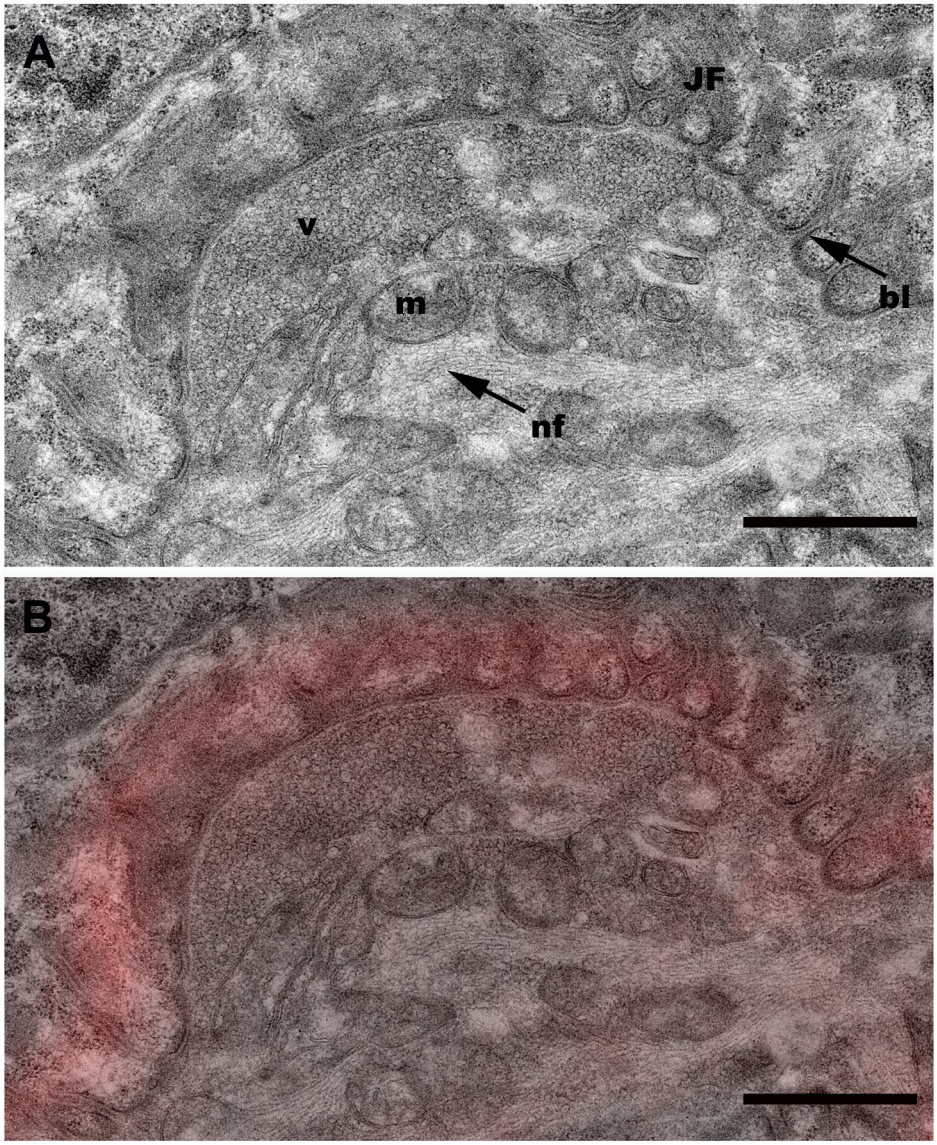

Fig. 6.

A. High magnification image of the region boxed in Fig. 5D showing additional morphological detail. bl, basal lamina; JF, junctional folds; m, mitochondria; nf, neurofilaments; v, vesicles. Scale bar= 1 μm. B. TEM-confocal overlay from the region boxed in Fig. 5D. Scale bar= 1 μm.